Intraband Radiometric Performance of the Landsat Thematic Mappers

Hugh H. Kieffer, Debra A. Cook, Eric M. Eliason, and *Patricia T. Eliason*
U.S. Geological Survey, Flagstaff, AZ 86001

ABSTRACT: Radiometric characteristics have been examined of the Landsat-4 and Landsat-5 Thematic Mappers (TMs) that can be established without absolute calibration of spectral data. This analysis is based on radiometrically and geometrically raw (B-type) data of both uniform (flat-field) and high-contrast scenes; most scenes were examined on an individual-detector basis. Subscences selected for uniform radiance were used to characterize subtle radiometric differences and noise problems. Although the general performance of the Thematic Mappers is excellent, we have quantified various anomalies that have a magnitude of a few digital levels (DN) or less. Virtually all of this imperfect performance is transferred into the fully processed (P-type) images, but it is disguised by the geometric resampling technique. Most of the imperfect performance could be corrected by ground processing; the computation cost would be least, and the accuracy retention greatest, if the correction were done immediately prior to the geometric resampling stage.

The effective resolution in radiance is degraded from its theoretical value by an average of 25 percent due to the irregular width of the digital levels. Histograms of aggregate scenes have been processed and a modulo-32 model developed to allow estimation of the width of all digital levels.

Several detectors exhibit a DC-level shift over a period of several scans; the largest shift is about 2 DN. There are two independent patterns of level shift for Landsat-4 and one for Landsat-5. Detectors switch simultaneously between states during scan-direction reversal, which can cause small apparent differences between forward and reverse scans for parts of an individual image.

All detectors in bands 1 and 2 in both TMs exhibit droop, a small offset that asymptotically decreases from the edge of the scene with a decay constant of about 1200 samples. In both TMs, some of the detectors in band 5 commonly overshoot high-contrast boundaries by several DN and require about 20 samples to recover.

When scanning across a bright target, Landsat-5 bands 2, 3, and 4 show an apparent offset of several DN, which decays in approximately 800 samples.

The high-frequency noise level of each detector is characterized by the standard deviation of the first difference in the sample direction across night scenes. Landsat-5 detectors are considerably more uniform within a band than those in Landsat-4. The average noise levels for the Landsat-4 TM reflective bands 1–5 and 7 range from 0.6 to 1.7 DN; those for Landsat-5 range from 0.3 to 1.4 DN.

Coherent noise was determined by Fourier transforms of uniform scenes. It was detectable only in Landsat-4 bands 1, 2, 3, and 4, and in Landsat-5 bands 1, 3, 5, and 7. For these bands, coherent noise common to most detectors has an average amplitude ranging from 0.1 to 0.5 DN in Landsat-4 and from 0.1 to 0.2 DN in Landsat-5; the amplitude for the most sensitive detector is typically twice the band average. The major periods of coherent noise in Landsat-4 are at 3.24 and 13.8 samples/cycle; in Landsat-5 these are at 4.7, 5.8, and 11.6 samples/cycle. The average amplitude of coherent noise for individual detectors reaches 0.6 DN for Landsat-4 (band 3, detector 1, 13.8 pixels/cycle) and 0.7 DN for Landsat-5 (band 5, detector 7, 11.6 pixels/cycle). The noise of longest period in both instruments is amplitude-modulated; the peak-to-peak amplitude reaches 5 DN in Landsat-4, detector 1 of band 3.

INTRODUCTION

SEVERAL INTRINSIC radiometric characteristics of the Landsat-4 and Landsat-5 Thematic Mappers (TMs) are discussed in this report. Our approach is based on examination of internal consistency within natural scenes rather than depending on calibration data. We emphasize that the overall behavior of the TMs is excellent; imperfect behavior is barely discernible in a typical image.

The study reported here is part of the Landsat Image Data Quality Analysis Program conducted by the National Aeronautics and Space Administration (NASA) (Salomonson and Koffler, 1983). Several related studies of the Landsat-4 TM are contained in a special issue of the *IEEE Transactions on Geoscience and Remote Sensing* (May 1984) and the reports of the Landsat-4 Early Results Symposium (NASA, 1984, 1985). Analyses covering aspects of TM performance similar to those reported here in-

PHOTOGRAMMETRIC ENGINEERING AND REMOTE SENSING,
Vol. 51, No. 9, September 1985, pp. 1331-1350.

0099-1112/85/5109-1331$02.25/0

clude those in the treatise by Barker (1984) and those of Bernstein *et al.* (1984), Malila *et al.* (1984), Kieffer *et al.* (1984), Metzler and Malila (1985), and Wrigley *et al.* (1985). Analyses by different investigators may yield somewhat different results, due more to variation in time of some TM characteristics and to the use of different scenes than to differences in analysis techniques.

TM data are available in three formats: raw (B-data), radiometrically corrected (A-data), and fully corrected (P-data). The only ground processing of B-data has been reformatting of the scene data to account for the bidirection scan, so that each line proceeds in the same direction; alternate scans generally are significantly offset. A-data are based on separate radiometric lookup tables for each detector for an entire scene. The lookup tables are derived from the detector response to internal-calibration light levels, and are constrained so that two input levels are never mapped into one output level. P-data result from geometrically resampling the A-data with a cubic convolution algorithm, utilizing spacecraft-position and -attitude information and, optionally, the positions of ground-control points.

Our approach has been to use data that could be available to the general Landsat digital-data customer, primarily the B-data (not a standard product) and P-data. The analyses presented here require neither the engineering nor internal-calibration data; we expect neither of these to be available from the National Oceanic and Atmospheric Administration (NOAA).

In using the A-data or B-data for statistical analysis, one must carefully correct the scan offset to ensure that the same scene areas are used for both forward and reverse scans. The geometric resampling technique employed in constructing the P-data makes impossible the recovery of the detector with which each pixel should be associated, and so these data cannot be used for studies of detector radiometry. We have characterized radiometric behaviors by their period or decay length in pixels. One pixel corresponds to 9.611 microseconds, from which the corresponding temporal frequency can be derived.

Thematic Mapper Operation

Because some concept of the operational mode of the TM is essential to understanding this study, a brief review is included here. More complete descriptions are available in Engle and Weinstein (1983), Salomonson and Koffler (1983), and Irons (1984).

The TM contains seven spectral bands. Bands 1 through 4 (0.45–0.52, 0.53–0.61, 0.62–0.69, and 0.77–0.91 μm, respectively) are spectrally adjacent bands in the visible and near-infrared, and the detectors are physically adjacent in the warm focal plane. The cold focal plane contains the detectors for bands 5 (1.57–1.78 μm) and 7 (2.10–2.35 μm) in the near-infrared spectrum and the detectors for band 6 (10.42–11.66 μm), which responds to thermal emission. In each band except band 6, 16 detectors are spaced by their own width in a direction normal to the scan direction. Within each band, the even- and odd-numbered detectors are on separate modules, spatially separated by 2.5 instantaneous fields of view in the scan direction. Band 6 contains four detectors, each of whose linear dimensions are four times as great as those of detectors in the other bands; these four detectors are also staggered. The sets of detectors in the seven bands are separated in the scan direction by 25 to 45 fields of view.

The TM actively gathers data in both directions of scan-mirror motion (16 lines of data are collected on the forward scan and 16 on the reverse). An optical scanline corrector converts into a rectangular pattern the saw-toothed scan pattern resulting from the motion of only the scan mirror and the spacecraft; both the forward and reverse scanlines in object space are virtually perpendicular to the spacecraft track. Some confusion can result from the fact that the formal numbering of the detectors is in reverse order from their relative position in the image, i.e., the last line of a scan is detector 1. In this study, the first 16 lines of a scene (the top lines, or the most northerly in daytime scenes) are taken to be in the forward direction, the next 16 lines in the reverse direction, and so forth.

DATA USED

The Landsat scenes used in this report are listed in Table 1. Our studies of both random and coherent noise have utilized, where possible, flat fields (areas of a scene with nearly constant radiance). In addition to nighttime scenes, we have included areas within Chesapeake Bay that are 512 pixels square or, where 1024 successive samples were within the

Table 1. Thematic Mapper Scenes Used in This Study. The first digit of the scene identification number indicates whether the scene was derived from Landsat-4 or Landsat-5

Location	Path/row	Date	Scene identification
Washington, DC	15/33	82 Nov 02	40109-15140
NE Arkansas	23/35	82 Aug 22	40037-16031
Cape Cod, MA	11/31	82 Dec 08	40145-14492
Roanoke, VA	114/210	82 Nov 08	40115-02364
Richmond, VA	112/210	82 Aug 22	40037-02230
NW Iowa	28/30	82 Aug 25	40040-16321
Gran Desierto, Mexico	38/38	83 Jan 06	40174-17392
Birmingham, AL	20/37	84 Mar 15	40608-15463
Birmingham, AL	20/37	84 Mar 15	50014-15460
White Sands, NM	33/37	84 Jul 18	50129-17075
San Francisco, CA	44/34	84 Jul 15	50126-18143
NW Iowa	28/30	84 Aug 06	50158-16350
Harrisburg, PA	111/212	84 Apr 16	50052-02182

bay, a marine section of the Cape Cod scene and two areas within San Francisco Bay. The two Birmingham scenes were acquired almost simultaneously by Landsat-4 and Landsat-5. The Gran Desierto and White Sands scenes were used to test data behavior over large contrast variations.

WIDTH OF THE DIGITAL LEVELS

Histograms of raw data for any daytime TM scene show a raggedness due to the large variation in the population of successive DN levels (see Figure 1). This jagged pattern of brightness population is the same for all detectors in a band, and the high-frequency part of this pattern repeats between scenes. Two obvious characteristics of this pattern are the overpopulation of approximately every fourth level and the common drastic underpopulation of level 127.

This behavior is attributed to nonuniform widths of successive voltage increments in the analog-to-digital converter (ADC) in the TM. The TM has a separate ADC for each band except band 5, through

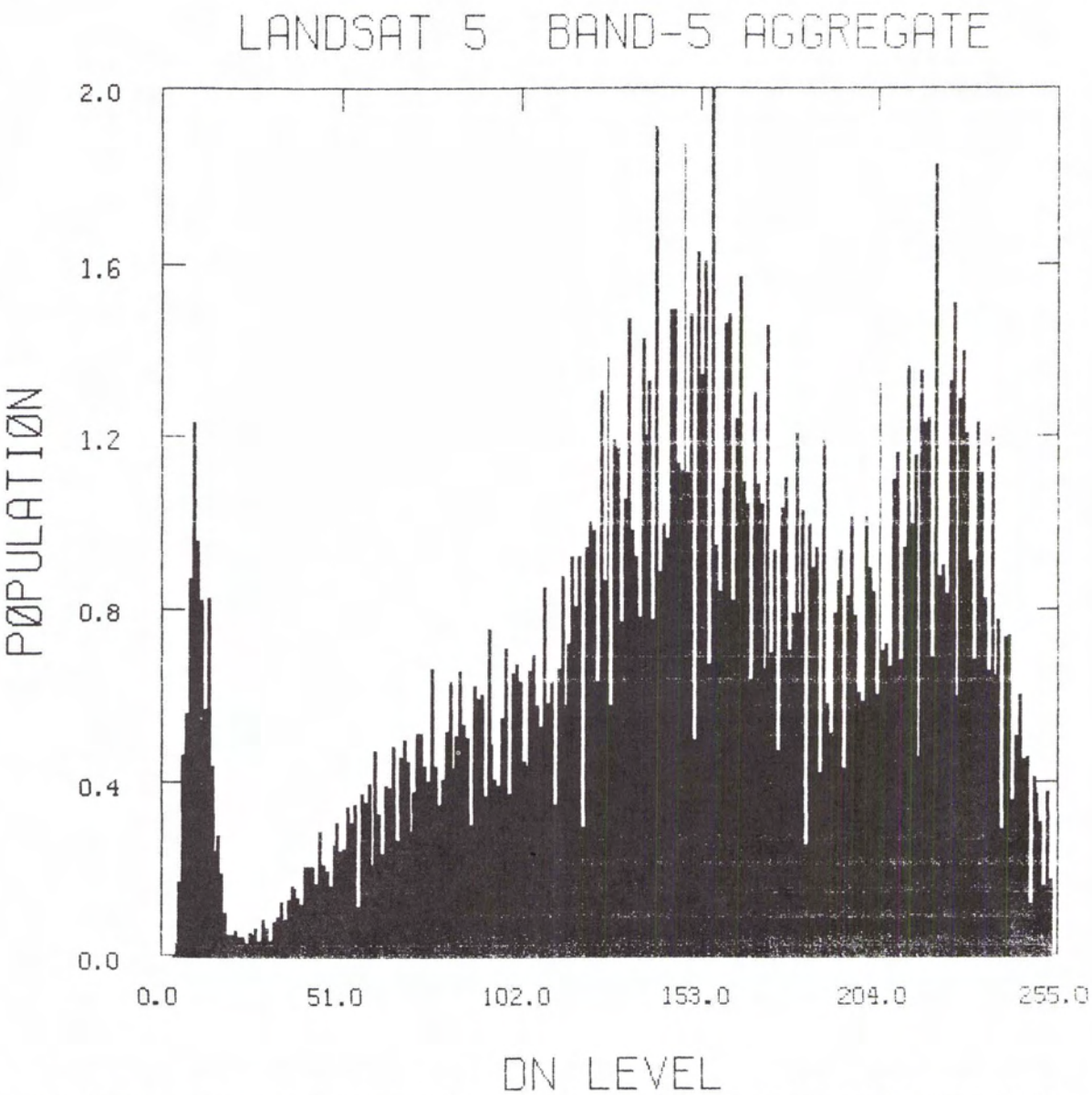

FIG. 1. Histogram of raw data of the Landsat-5, band 5, aggregate scene. The population scale factor is 150,000. The ragged appearance is due to large variation in adjacent intervals and is characteristic of the TM raw data.

whose ADC the data for the thermal band are processed. These effects are consistent in B-data, but they may be shifted in level by the radiometric equalization used in generating A-data. This behavior is masked in P-data by geometric resampling.

To quantify this behavior for Landsat-5, we added together, for each band, histograms of multiples of 128 lines (full width or quad width) of raw data from several scenes selected for their wide aggregate range in brightness. This addition yielded a broad population. These multiscene histograms were then filtered with a triangular filter of full-width nine (1/5, 2/5, etc.) to yield a distribution that would approximate the actual brightness population in the aggregate natural scene. We then divided the raw aggregate histogram by the filtered aggregate histogram to obtain the normalized abundance of all digital levels (Figure 2). The relative narrowness of scene histograms of the thermal band prevented generation of a wide aggregate histogram for band 6. The filtering technique tends to underemphasize the variation of individual levels (because they have

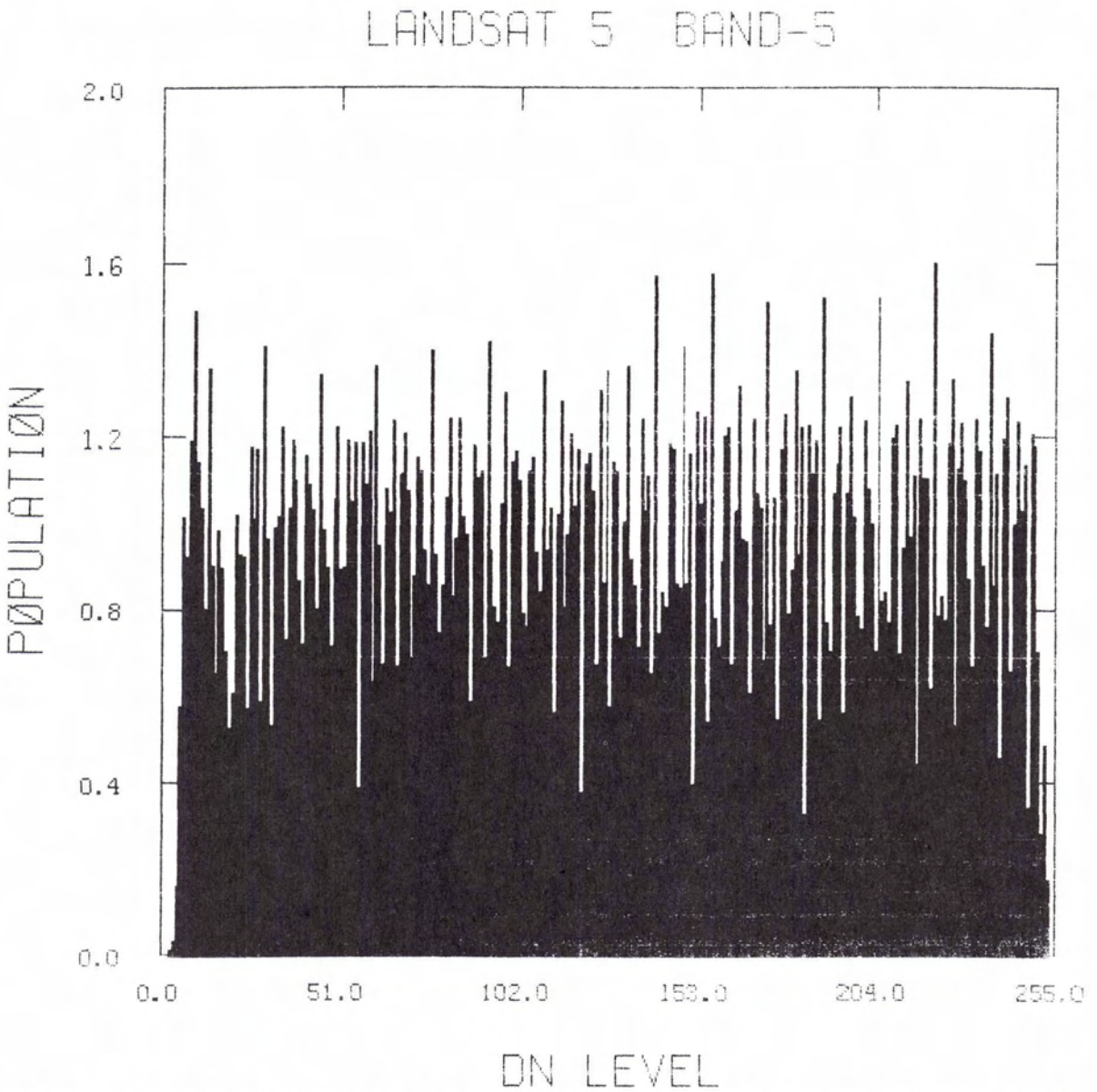

FIG. 2. Normalized aggregate histogram for Landsat-5, band 5. The raw-aggregate histogram was smoothed with a triangular filter and the smoothed histogram then divided into the raw histogram. Population shown represents effective width of each quantization level. The patterns for each interval of 32 levels are somewhat consistent.

the greatest weight in the filter) and raises/lowers the attributed width for levels near large negative/positive second derivatives in the aggregate histogram. Although a more elaborate filtering technique to estimate the actual brightness population might improve the quantization-width estimates, tests with a triangular filter of full-width five and Gaussian filters yielded only minor differences.

The periodicity of the normalized abundance pattern suggested the modelling of the spacecraft electronics on the basis of a successive-approximation ADC. In such a model, the width of a digital level is assumed to be directly related to the differences of two successive comparison voltages, which are in turn the sum of a set of reference voltages based on successive powers of 2. This model failed to reproduce the observed populations except the overpopulation of every fourth level. Such failure is due to the lack of detailed repetitiveness of the pattern; a successive-approximation model predicts the same relative abundance of, for instance, levels 4, 12, 20, 28, etc.

The normalized populations suggest a repetitive pattern of length 32. To quantify this repetition, the successive intervals of 32 levels for each band were folded onto one another, excepting the extreme levels that have inadequate statistics. The resulting population (Figure 3) shows considerable regularity

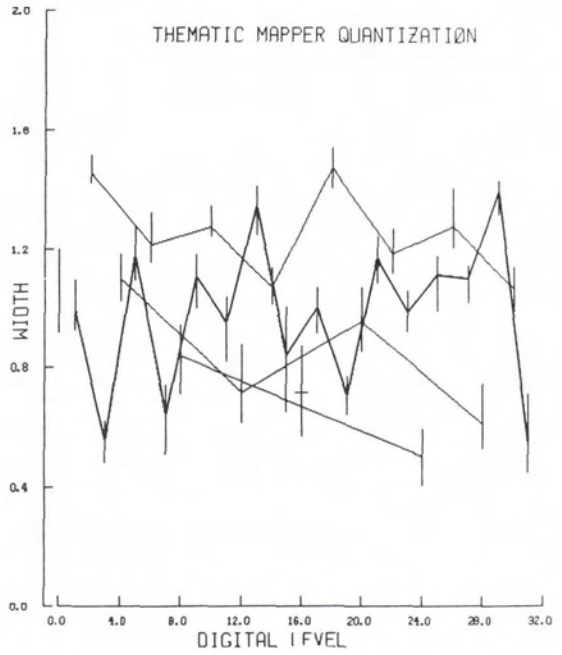

FIG. 3. Width of the TM quantization levels in Landsat-5, band 1, based on a modulo-32 grouping, using a total range of 94 to 248 DN. Vertical lines indicate the range of width for each modulo-32 group. Average values are connected on the basis of the largest integral divisor which is a power of 2. The pattern is similar for the other TM bands.

when levels are grouped according to their maximum divisor that is a power of 2 (the highest power of 2 that changes in creating that level, *i.e.*, the most significant bit). Within the interval of 32 are several patterns: each set oscillates regularly, with the first member of a set being higher than the second; the 2's levels (2, 6, 10, etc.) have a greater average width than all other sets; the pattern repeats at modulo-16 (but some ranges would then not overlap); the least consistent modulo-32 levels are 0, 31, 16, and 15.

These basic patterns are similar in all six reflective bands. The repetition in the bands, and the consistency among the various intervals of 32 levels, suggest that this nonuniformity of the ADC is generic to the electronic design. The least consistent bands are 5 and 6, which share an ADC (see bottom four rows of Table 2). The additional speed required of the shared ADC thus may have significantly affected its performance. Although these bands share an ADC, their width patterns are not consistent. For example, level 143 is 1.08 and 0.20 times the width of adjacent levels in bands 5 and 6, respectively.

The actual response boundary between successive DN levels was determined by forming the cumulative sum of the average at each level in the 32 intervals (Table 2). The mean difference of these cumulative sums from the appropriate integer is one quantitative measure of the proportion of pixels that are assigned to the wrong digital level (see Table 2, row C). Another measure, not sensitive to cumulative errors, is the mean absolute deviation of the normalized widths from 1.0 (Table 2, row D). Both measures indicate that about 20 percent of the level assignments of TM on Landsat-5 should be in an adjacent level. The most significant deviations occur at digital levels that are multiples of, or one less than a multiple of, 32.

The aggregation of scenes to form a broad histogram was not carried out for Landsat-4, whose population patterns are similar to those of Landsat-5 except that DN level 127 is nearly absent in some bands, being underpopulated by a factor greater than 10.

These results can be used in conjunction with an absolute calibration, or the eight-level internal calibration, to adjust the precise response attributed to each DN level. Such a correction could be incorporated at the resampling stage of generation of P-data with virtually no computation cost. Histograms of raw data can also be cosmetically corrected through use of the values given in Table 2.

LEVEL SHIFT

Images made from raw TM data commonly show brightness variation in bands whose width is a multiple of 16 lines. Examination of data on an individual-line basis reveals a shift of the average for all detectors during some scan reversals (outside the

TABLE 2. WIDTHS OF LANDSAT-5 THEMATIC MAPPER QUANTIZATION LEVELS

THE UPPER PORTION OF THE TABLE LISTS THE CUMULATIVE WIDTH MODULO-32, NORMALIZED TO TOTAL 31. THE NEXT SET OF ROWS LISTS THE WIDTHS OF THE LEVELS WHICH ARE A MULTIPLE OF 32. THE LAST FOUR ROWS ARE STATISTICAL SUMMARIES:

A: STANDARD DEVIATION OF WIDTHS OF LEVELS WITHIN THE STATED RANGE.

B: AVERAGE OF THE STANDARD DEVIATIONS OF WIDTHS IN EACH OF THE 31 LEVELS.

C: AVERAGE DEVIATION OF THE CUMULATIVE 31 LEVELS FROM THE APPROPRIATE INTEGER.

D: AVERAGE DEVIATION OF THE 31 WIDTHS FROM 1.0

	Band 1	Band 2	Band 3	Band 4	Band 5	Band 6	Band 7
Min DN	94	49	24	24	4	76	11
Max DN	248	237	250	250	254	165	176
Cumulative width							
1	0.99	0.97	1.08	0.82	1.13	0.88	0.93
2	2.45	2.32	2.36	2.20	2.39	1.71	2.28
3	3.00	3.06	3.02	2.99	3.06	2.17	3.05
4	4.09	4.17	4.12	4.07	4.04	3.09	4.09
5	5.27	5.30	5.32	4.99	5.23	4.23	5.18
6	6.49	6.51	6.44	6.31	6.28	5.61	6.39
7	7.12	7.03	7.13	6.85	7.14	6.43	6.98
8	7.96	7.98	7.89	7.92	7.94	7.63	7.97
9	9.06	9.10	9.09	8.86	9.20	9.04	8.99
10	10.33	10.27	10.23	10.14	10.33	10.11	10.22
11	11.28	11.27	11.15	11.13	11.35	11.06	11.20
12	11.99	12.05	11.93	12.01	12.13	11.95	11.96
13	13.33	13.38	13.37	13.18	13.59	13.21	13.22
14	14.40	14.43	14.29	14.34	14.48	14.14	14.31
15	15.24	15.29	15.23	15.18	15.40	14.54	15.16
16	15.95	15.89	15.81	15.97	16.12	15.81	15.93
17	16.95	16.90	16.90	16.86	17.24	17.04	16.92
18	18.42	18.20	18.18	18.25	18.44	18.30	18.26
19	19.12	19.10	18.99	19.21	19.22	19.33	19.12
20	20.07	20.06	19.94	20.15	20.13	20.39	20.03
21	21.24	21.19	21.16	21.14	21.40	21.66	21.17
22	22.42	22.36	22.24	22.38	22.40	22.67	22.31
23	23.40	23.27	23.31	23.25	23.53	23.45	23.23
24	23.90	23.83	23.71	23.99	23.97	24.00	23.84
25	25.01	24.97	24.90	24.95	25.19	25.12	24.92
26	26.29	26.10	26.06	26.17	26.32	25.98	26.13
27	27.39	27.35	27.26	27.33	27.44	27.20	27.31
28	28.00	27.91	27.82	28.00	28.03	28.12	27.89
29	29.39	29.25	29.31	29.22	29.39	29.74	29.19
30	30.45	30.30	30.21	30.32	30.18	30.69	30.24
31	31.00	31.00	31.00	31.00	31.00	31.00	31.00
0							
32			0.65	0.41	0.54		0.71
64		0.49	0.50	0.66	0.69		0.76
96	0.71	0.79	0.92	0.70	0.83	0.43	0.85
128	0.45	0.97	1.12	1.13	1.38	0.48	0.89
160	0.46	0.61	0.81	0.54	0.73		0.61
192	0.51	0.51	0.56	0.67	0.72		
A	0.278	0.248	0.277	0.224	0.278	0.400	0.226
B	0.074	0.070	0.093	0.070	0.137	0.247	0.071
C	0.225	0.193	0.215	0.180	0.198	0.229	0.177
D	0.210	0.191	0.183	0.154	0.253	0.330	0.154

scene data). Some detectors are significantly more sensitive to this level shift than are others: Landsat-4 appears to have two patterns of sensitivity, and Landsat-5 has one. Although in some instances the level shift correlates with the forward-reverse phase of the scan, it more commonly has an irregular and somewhat longer period (see Figure 4 and Plate 1; and Malila *et al.*, 1984, Figures 13 to 16).

Although for the most sensitive detectors the line average is adequate to determine the phasing of the level shift, for the less sensitive detectors it is not adequate, especially for daytime scenes. To estab-

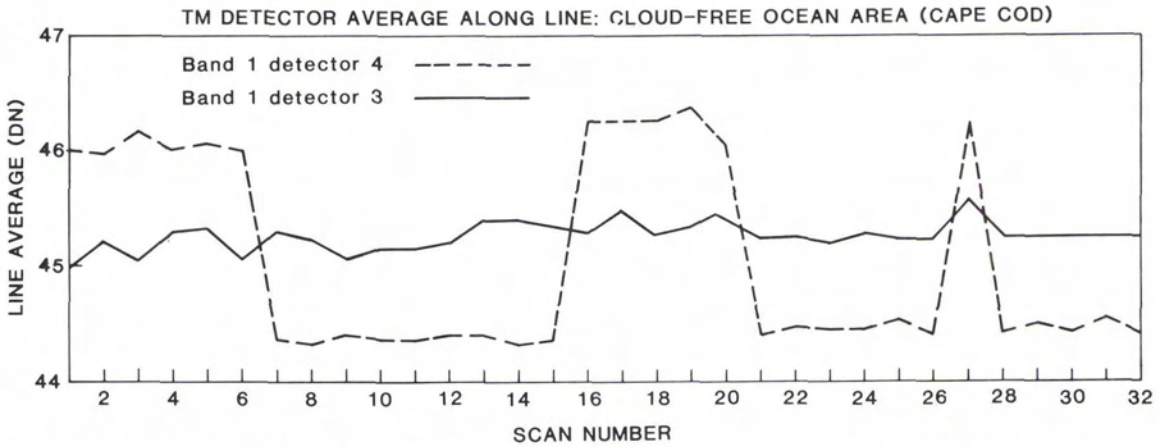

FIG. 4. DN line average of two adjacent Landsat-4 detectors (3 and 4, band 1) in the Cape Cod, MA, scene as a function of scan number, showing TM detector-level shift. Detector 4 is an extreme case of level shift; detector 3 is more typical.

lish the shift pattern and to determine the sensitivity for all detectors, line averages were taken across entire quadrants or scenes. The shift state of each scan was established by comparing one or more sensitive detectors with adjacent insensitive detectors for each pattern. The most consistent level-shift patterns from scene to scene were produced by Landsat-4, band 1, detectors 3 versus 4 (pattern A); Landsat-4, band 7, detectors 7 versus 8 (pattern B); and Landsat-5, band 2, detectors 1 and 3 versus 2 and 4.

First, a histogram of this difference was made for a large set of scans; this histogram is bimodal, usually with an empty central section. Then a trigger level was chosen between the two modes and used to assign the level-shift state for each scan in a particular scene. This technique proved reliable for all test scenes except those containing extreme contrast, e.g., the Gulf of Mexico and adjacent sand dunes. For these exceptions, the trigger level used to assign level-shift state had to be reset at the contrast boundary.

The level-shift sensitivity for each detector was then quantified by grouping into two sets, depending on level-shift state, the values of line-average offset for that detector. The reference level for this offset is the average for all detectors in that scan, corrected for the average level shift of the band (if the scan is in a shifted state), and linearly interpolated between scan centers. The mean and standard deviations of each set were then computed. The level-shift sensitivity of a detector is defined as the difference between these two means. The standard deviation of the level shift for a detector is defined as the RMS sum of the standard deviations of the two states.

The amplitude of the level shift may be slightly sensitive to brightness of the scene (see Table 3). Level-shift sensitivities were determined for all detectors for four Landsat-5 scenes (the two listed in Table 3 plus northwest Iowa and White Sands): the sensitivities of detectors within each band are little changed relative to one another. Band 5 exhibits the greatest change between scenes. The two Landsat-4 level shifts occur independently: pattern B, strongest in band 7, switches frequently; pattern A, strongest in band 1, may hold one state for many successive scans. Landsat-5 is somewhat less sensitive to level shift.

The level-shift standard deviations of the Birmingham daytime scene are strongly correlated with the standard deviation of the raw data and are generally larger than the level shift itself. A comparison of the day and night level-shift sensitivity computations indicates that the day determination is reliable to approximately one-fourth of the level-shift standard deviation, i.e., to about 0.1 DN. The sensitivity of each detector to level shift is most reliably determined in a night scene; the level-shift standard deviation for all reflective bands for the Harrisburg night scene is 0.01 to 0.03 DN.

In most bands, the sign of the sensitivity to level shift oscillates between even- and odd-numbered detectors, corresponding to the detector module on which they are mounted (see Figure 5). Detectors toward the ends of the modules are generally more sensitive to level shift.

The recommended correction procedure is to use (1) detector sensitivities determined from contemporary night scenes or the values in Table 3, and (2) the level-shift state determined for each scan based on the reference detectors and day-scene trigger level. Level shift can be separated from droop (see next section) when using only a quarter scene, as level-shift sensitivity varies greatly among detectors and droop is reasonably independent of detector in

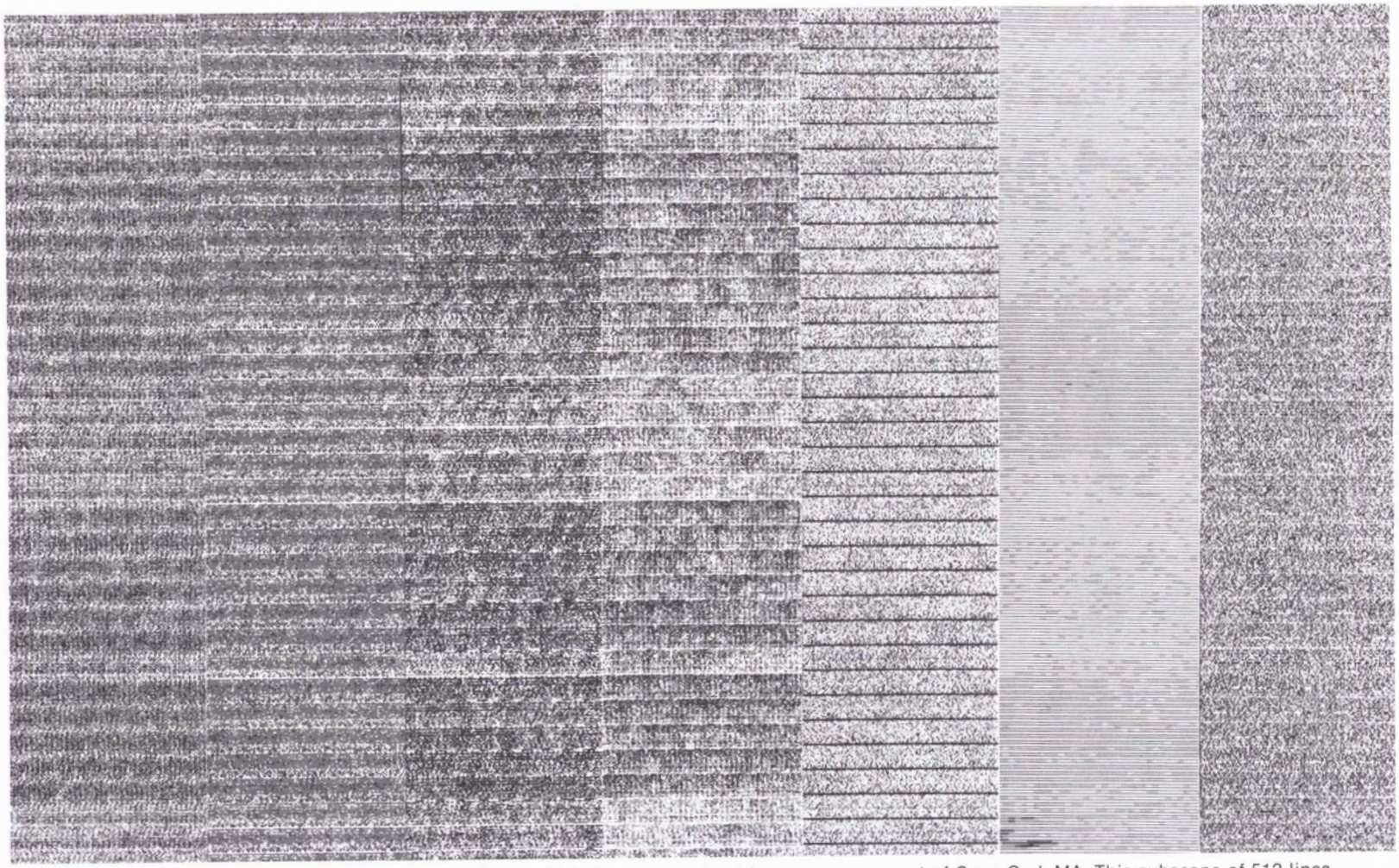

PLATE 1. Mosaic of seven bands of the Landsat-4 TM B-data over a cloud-free ocean area east of Cape Cod, MA. This subscene of 512 lines and 100 samples provides a uniform-radiance target used for graphic display of random- and coherent-noise level. Each band was contrast enhanced to maximize visual inspection. Black-to-white DN levels are 41-50 for band 1 (left), 12-17 for band 2, 10-14 for band 3, 5-9 for band 4, 2-7 for band 5, 87-92 for band 6, and 0-7 for band 7 (right). High-frequency graininess of bands 1, 3, and 4 is attributed to large amplitudes of 3.26 pixels/cycle coherent noise. "Stitching" pattern in band 3 results largely from coherent noise in detector 1 of 13.8 pixels/cycle. Black lines in band 5 are due to dead detector 3. Detector 7 in band 7, which has the largest noise level, stands out visually as random alternation between black and white within a line. Between-band correlation of level shift is visible as dark and light strips that span bands, an effect most evident in bands 1, 3, and 4.

TABLE 3A. SENSITIVITY OF DETECTORS TO LEVEL SHIFT
LANDSAT-4 A & B 40608-15463 — BIRMINGHAM, AL — QUAD 2
LANDSAT-5 50014-15460 — BIRMINGHAM, AL — QUAD 2
LANDSAT-5 NIGHT 50052-02182 — HARRISBURG, PA — QUAD 1

	Band-Averaged Values for Each Level-Shift Pattern									
	Absolute Level Shift				Standard Deviation				Data Number	
	4A	4B	5	5 night	4A	4B	5	5 night	4	5
Band 1	0.57	0.07	0.23	0.15	0.31	0.53	0.26	0.03	70.12	74.47
Band 2	0.15	0.13	0.24	0.14	0.19	0.18	0.18	0.01	28.66	30.72
Band 3	0.34	0.27	0.32	0.31	0.35	0.30	0.29	0.01	31.21	33.87
Band 4	0.16	0.07	0.12	0.09	0.41	0.41	0.39	0.01	46.92	47.67
Band 5	0.17	0.14	0.14	0.08	0.88	0.87	0.86	0.02	76.47	75.76
Band 6	0.03	0.04	0.01	0.07	0.20	0.20	0.11	0.14	134.58	103.82
Band 7	0.15	0.31	0.09	0.08	0.52	0.46	0.45	0.02	33.63	33.33

TABLE 3B. SENSITIVITY OF INDIVIDUAL DETECTORS TO LEVEL SHIFT
LANDSAT-4 A & B 40608-15463 — BIRMINGHAM, AL — QUAD 2
LANDSAT-5 50014-15460 — BIRMINGHAM, AL — QUAD 2
LANDSAT-5 NIGHT 50052-02182 — HARRISBURG, PA — QUAD 1

	Individual detector sensitivity					*Individual detector sensitivity*			
	4A	4B	5	5 night		4A	4B	5	5 night
Band-Detector					Band-Detector				
1- 1	0.77	−0.20	−0.04	0.03	3- 1	0.69	−0.61	0.47	0.47
1- 2	0.16	−0.08	−0.30	−0.23	3- 2	0.34	0.36	0.28	0.20
1- 3	0.21	−0.07	−0.04	0.05	3- 3	0.40	−0.27	0.46	0.43
1- 4	2.24	0.11	−0.32	−0.19	3- 4	0.16	0.08	0.44	0.39
1- 5	0.16	−0.12	−0.12	0.04	3- 5	0.46	−0.23	0.30	0.31
1- 6	0.42	0.03	−0.36	−0.26	3- 6	0.38	0.11	0.38	0.34
1- 7	0.04	−0.02	0.00	0.11	3- 7	0.32	−0.23	0.28	0.29
1- 8	1.10	−0.10	−0.31	−0.21	3- 8	0.04	0.00	0.14	0.15
1- 9	0.01	0.14	−0.09	0.04	3- 9	0.10	−0.08	0.28	0.33
1-10	1.27	0.00	−0.47	−0.30	3-10	0.33	0.14	0.24	0.25
1-11	−0.04	0.05	−0.02	0.07	3-11	0.21	−0.17	0.32	0.37
1-12	1.91	0.02	−0.49	−0.21	3-12	0.21	0.26	0.20	0.34
1-13	0.24	0.02	−0.15	−0.01	3-13	0.44	−0.21	0.41	0.32
1-14	0.42	−0.01	−0.42	−0.31	3-14	0.34	0.23	0.28	0.25
1-15	0.10	−0.05	−0.12	0.00	3-15	0.54	−0.45	0.39	0.32
1-16	0.02	0.04	−0.37	−0.27	3-16	0.45	0.86	0.27	0.26
Band-Detector					Band-Detector				
2- 1	0.38	−0.39	0.48	0.52	4- 1	0.25	−0.02	0.29	0.28
2- 2	0.21	0.09	0.10	0.09	4- 2	0.09	−0.05	0.21	0.15
2- 3	0.03	−0.16	0.31	0.24	4- 3	0.20	−0.03	0.17	0.15
2- 4	0.15	−0.14	−0.10	−0.01	4- 4	0.03	−0.10	0.32	0.20
2- 5	0.15	−0.14	0.35	0.18	4- 5	0.22	−0.06	0.16	0.04
2- 6	0.16	0.05	0.19	0.07	4- 6	0.19	−0.08	0.02	0.05
2- 7	0.06	−0.10	0.26	0.15	4- 7	0.13	−0.08	0.05	0.03
2- 8	0.16	0.04	0.14	0.07	4- 8	−0.06	−0.13	−0.11	0.01
2- 9	0.12	−0.10	0.22	0.08	4- 9	0.09	0.00	0.01	0.08
2-10	0.14	0.09	−0.01	0.02	4-10	0.13	0.04	−0.12	0.01
2-11	0.06	−0.06	0.20	0.09	4-11	0.16	0.06	0.02	0.10
2-12	0.05	0.08	0.04	0.02	4-12	0.30	0.11	−0.12	0.02
2-13	0.19	−0.14	0.34	0.17	4-13	0.17	0.05	0.12	0.14
2-14	0.19	0.07	0.31	0.08	4-14	0.07	0.07	−0.04	0.08
2-15	0.21	−0.19	0.28	0.16	4-15	0.19	0.07	0.08	0.08
2-16	0.15	0.17	0.50	0.26	4-16	0.27	0.14	−0.07	0.01

[TABLE 3B—*Continued on Next Page*]

TABLE 3B.—*Continued*

	Individual detector sensitivity					Individual detector sensitivity			
	4A	4B	5	5 night		4A	4B	5	5 night
Band-Detector					6- 3	−0.01	−0.01	−0.01	−0.03
5- 1	0.10	−0.07	0.36	0.14	6- 4	0.02	−0.05	−0.01	0.07
5- 2	0.30	−0.15	0.39	0.00					
5- 3	0.39	−0.06	0.48	0.19	Band-Detector				
5- 4	0.39	−0.06	0.26	−0.02	7- 1	0.10	0.23	0.11	0.01
5- 5	−0.03	−0.06	0.10	−0.07	7- 2	0.19	−0.35	0.17	−0.01
5- 6	0.36	−0.15	0.07	−0.13	7- 3	0.05	0.30	0.07	−0.05
5- 7	0.17	0.10	0.08	0.01	7- 4	0.27	−0.27	0.00	−0.11
5- 8	0.15	−0.27	0.04	−0.12	7- 5	0.09	0.33	0.07	0.00
5- 9	−0.01	0.12	0.06	0.06	7- 6	0.29	−0.28	−0.05	−0.09
5-10	−0.08	0.88	0.08	0.01	7- 7	0.02	1.02	0.17	0.15
5-11	0.00	0.16	−0.01	0.10	7- 8	0.19	−0.32	−0.12	−0.16
5-12	0.20	0.13	−0.20	−0.12	7- 9	−0.04	0.26	0.18	0.16
5-13	−0.03	0.05	−0.04	0.02	7-10	0.14	−0.38	−0.19	−0.15
5-14	0.10	0.00	−0.02	−0.08	7-11	0.00	0.32	0.03	0.11
5-15	−0.16	−0.04	−0.09	−0.09	7-12	0.29	−0.20	−0.10	−0.06
5-16	0.19	0.00	−0.01	−0.14	7-13	0.00	0.23	0.00	0.03
Band-Detector					7-14	0.33	−0.08	−0.07	−0.04
6- 1	0.02	−0.06	0.01	−0.08	7-15	0.04	0.23	0.01	0.02
6- 2	0.05	−0.02	0.01	0.09	7-16	0.32	−0.17	−0.07	−0.12

a band; also, droop is rigorously related to scan direction, whereas level shift is irregular. If calibration lamp data are available, they can be used for a simpler determination of level-shift state (Malila *et al.*, 1984).

DROOP

Thematic Mapper scenes commonly show strongest scan striping near the ends of scan lines. Earlier studies (Kieffer *et al.*, 1984; Malila *et al.*, 1984) indicated that the TM response asymptotically approaches a uniform level as it scans into a scene, and that the magnitude of this effect depends on scene radiance. In order to compare the behavior of Landsat-4 and Landsat-5, the data for all detectors in bands 1 and 2 were averaged in sets of 64 samples, in the scan direction, for each scan line in the top half of the Birmingham scene. The average values for the adjacent forward and reverse scans were subtracted to generate an average forward-minus-reverse difference. The resulting data were assumed to be symmetric about the middle of a scan, and to have the form:

$$Ae^{-S/B}$$

where S is the number of samples from the edge of the scene in the scan direction. The results are listed in Table 4. The uncertainties in A and B are approximately 0.01 and 50, respectively. The Landsat-4 values agree with those determined previously for scenes with comparable radiance (Iowa and Cape Cod, band 1) (Kieffer *et al.*, 1984). In night scenes (average DN, 2 or 3) and in the Cape Cod ocean scene (band 2 DN, 14; band 3 DN, 12), the droop was found to be less than 0.1 DN and probably less than 0.05 DN.

This effect is probably proportional to the average radiance in the scene relative to the radiance that occurs during some aspect of the complex calibration and reset sequence during scan reversal (see Barker, 1984; Barker *et al.*, 1984a). Nonetheless, a good approximation of droop can be determined from natural-scene data alone.

OVERSHOOT

Some of the detectors in band 5 of both Landsat-4 and Landsat-5 exhibit an overshoot response when scanning across an abrupt boundary between two spatially large areas of significantly different average-brightness levels; the detectors overestimate (overshoot) the change in brightness level for a finite time before recovering to the proper level. The visible effect of overshoot can be seen when the detectors scan from bright terrain to dark water of uniform brightness (Plate 2). On the water side of the boundary, some of the detectors will appear darker than neighboring detectors.

The overshoot effect was examined on the Landsat-4 Washington, DC, scene and the Landsat-5 White Sands scene. In the Landsat-4 scene (Plate 2), when the scanner crossed from land (average DN, 55) to water (average DN, 5), detectors 1, 2, 15, and 16 overshot the change in brightness level; thus their DNs are initially lower than the average value of the bay. The overshoot effect diminishes and completely disappears over a scan length of 30

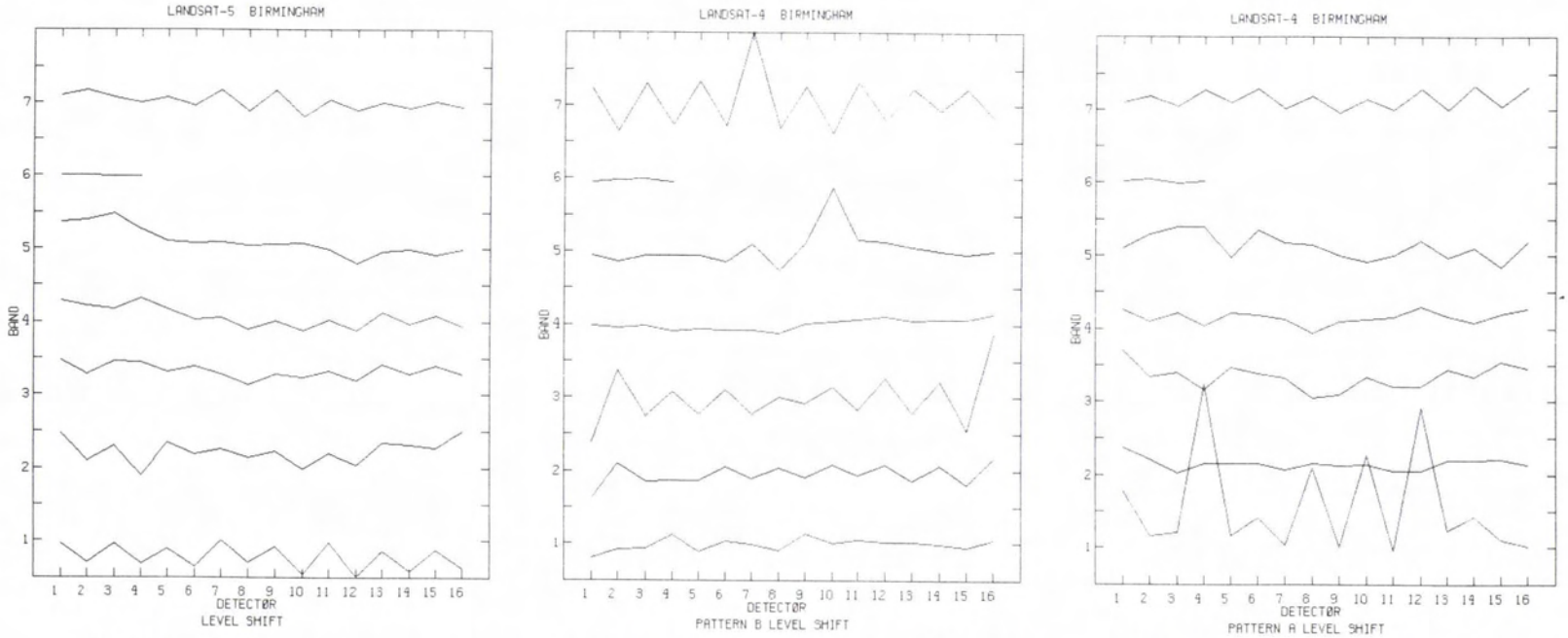

FIG. 5. Level-shift sensitivity of the TM detectors for the Birmingham scene. The scale is 0.5 DN per division. Part a; Landsat-4, pattern A. Although the sensitivity oscillates between even- and odd-numbered detectors, corresponding to the two detector modules per band, the average shifts for each band are in phase. Part b; Landsat-4, pattern B. The average shift for each band is near zero. Part c; Landsat-5. The average shift for band 1 is out of phase with the other bands.

pixels from the boundary. To quantify this effect, the first 15 pixels of the water at the terrain boundary were averaged and compared with representative water values for each detector in the forward and reverse scan directions. Detector 1 was found to be lower by an average of 0.47 DN, detector 2 by 0.73 DN, detector 15 by 0.78 DN, and detector 16 by 0.62 DN; the effect for the other 12 detectors was negligible.

In the Landsat-5 scene, when the scanner crossed from land (average DN, 126) to water (average DN, 5.5), detectors 15 and 16 exhibited a 1.5-DN average overshoot that disappeared over a scan length of 50 pixels from the boundary. A similar behavior of smaller magnitude was noted in band 7.

In each band, the detectors most sensitive to this effect are near the ends of the detector arrays; their behavior can be characterized as an overshoot of about 1.5 percent with an asymptotic decay constant of about 20 pixels. An overshoot common to all detectors, with a decay length of about 70 samples, has been reported by Fusco *et al.* (1985).

DELAY IN BRIGHT-TARGET RECOVERY

Bright-target recovery is the ability of the TM detectors to return to their normal sensitivity after scanning over an extended area that is at or near saturation levels. Bright-target recovery delay (BTRD) has been reported (Fischel, 1984; Santa Barbara Research Center, 1984) for both Landsat-4 and Landsat-5 TMs. It appears as dark stripes extending from bright areas on alternate scans.

The Landsat-5 TM scene of the San Francisco Bay area (Plate 3) illustrates the effect of BTRD. This scene has heavy cloud cover over the Pacific Ocean and eastward over the Pacific Coast Range extending into part of the populated bay area; the bay itself and areas to the east are largely cloudfree except for a small area approximately 150 pixels wide along the east edge of the bay. The dark stripes in the southern part of the bay correspond to the forward scan direction and the light stripes to the reverse scan direction. In the forward direction, the detectors have passed over a large area of bright cloud cover that diminished their sensitivity before they passed over the bay.

To quantify BTRD, adjacent forward and reverse scans over water (a first-order flat field) were compared as a function of distance from the east edge of the cloud. The minimum separation between the cloud edge and the bay is approximately 100 pixels; separation increases toward the south to a maximum of 800 pixels. The cloud edge is not sharp, and the uncertainty in consistent determination of its position is estimated to be about 30 pixels. The data for each scan were averaged into boxes of 16 lines by 50 samples eastward across the bay, excluding areas that apparently contain objects in the water. The differences between the average DN for the corresponding forward and reverse boxes were plotted as a function of distance from the cloud edge for 20 scan pairs (Figure 6). Data adequate to characterize the BTRD were obtained for distances of 100 to 1000 pixels from the cloud. The reverse scan direction, which did not pass over cloud cover, is assumed to contain no BTRD. Bands 2, 3, and 4 showed the forward scan direction to be several DN lower than the reverse scan direction near the cloud edge (see Table 5); the detectors recovered to within less than 0.5 DN of normal response at a distance of 800 pixels from the cloud edge. The scatter in the data caused by brightness variation in the cloud and in the bay (due to sediment load) does not allow a confident determination of the shape of the BTRD, but it is expected to be asymptotic. The BTRD in bands 1, 5, and 7 is less than 0.25 DN in this scene.

No striping is apparent within the cloud; visual examination of contrast-enhanced images suggests that it is less than 1 DN. The land-water contrast in band 4 of about 50 DN is just adequate to cause detectable BTRD in reverse scans along the east edge of the northern part of the bay, a distance of more than 1800 pixels from the edge of the clouds along the ocean coast. No detectable BTRD is associated with the isolated, small, bright cloud near the east edge of the bay. Thus, the magnitude of the BTRD effect depends both on the relative contrast between the bright and dark targets and on the extent of the bright target.

TABLE 4. DROOP MEASURED IN THE BIRMINGHAM SCENE. A IS THE MAGNITUDE AT SCENE EDGE. B IS THE EXPONENTIAL LENGTH IN SAMPLES (SEE TEXT)

		A	B	Average DN
Landsat-4	Band 1	1.05	1150	71.21
	Band 2	0.22	1350	28.79
Landsat-5	Band 1	0.54	1100	74.78
	Band 2	0.23	1200	30.97

NOISE

The random and coherent noise levels for all detectors in both TMs were determined by examining flat-field natural scenes, either night scenes or those of large expanses of water. Examples of noise are shown in Plate 1. The B-data for band 6 were decimated by a factor of four in both directions to undo the four-fold replication procedure involved in constructing the computer-compatible tapes; this decimation recovers the initial behavior of the detectors.

RANDOM, HIGH-FREQUENCY DETECTOR NOISE

The noise level of each detector was obtained by computing the first difference between adjacent samples and then determining the standard deviation of the first difference for each detector in the

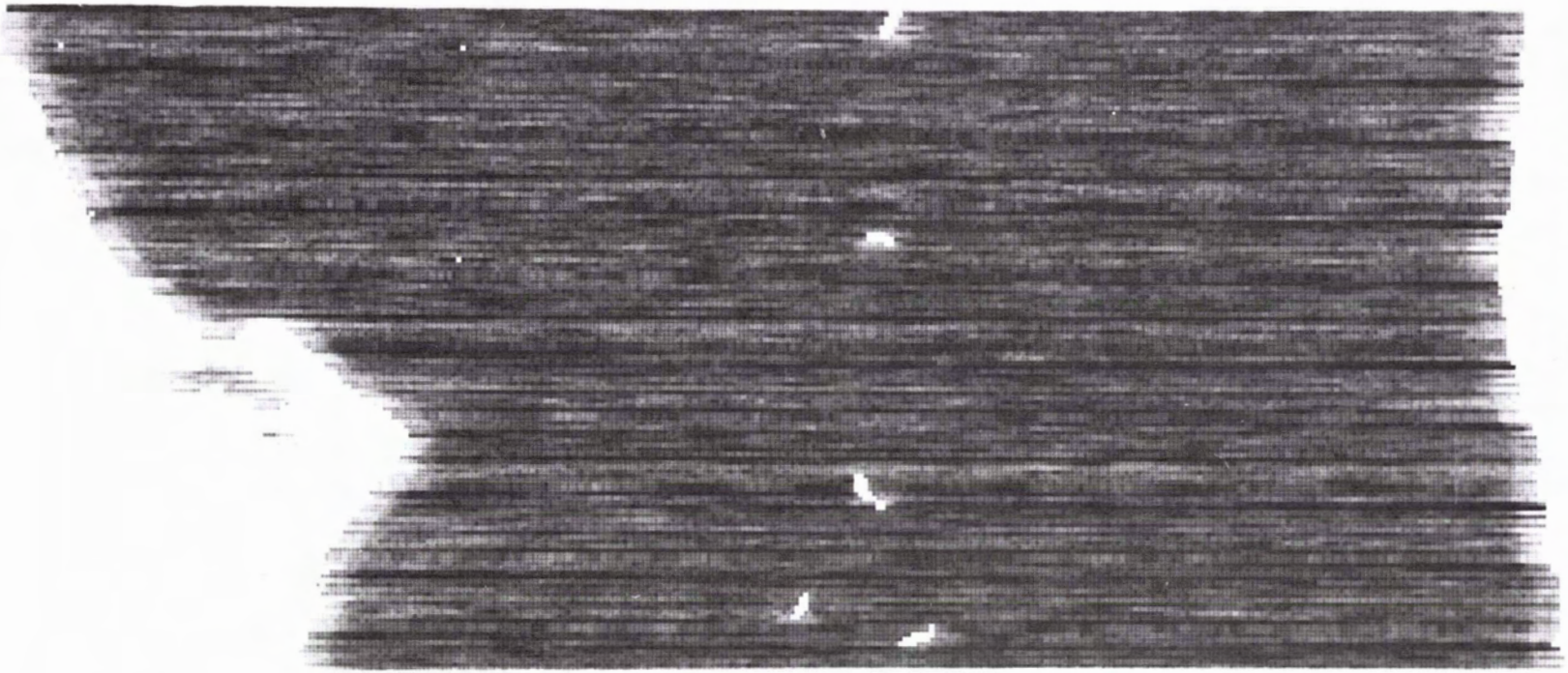

PLATE 2. A 216 × 512 Landsat-4 subscene in Chesapeake Bay area of Washington, DC, frame, showing overshoot response in detectors 1, 2, 15, and 16 of band 5. For this example, the DN values were first multiplied by 5 (to preserve fractional DN values in the averaging process), and then a rectangular filter, 11 pixels long, was applied along the scan lines in water areas of the subscene. Overshoot effect is visible along border between land (saturated in white) and water (darker areas). Visibility of this effect on both sides of the bay indicates that the effect exists in both forward and reverse scan directions.

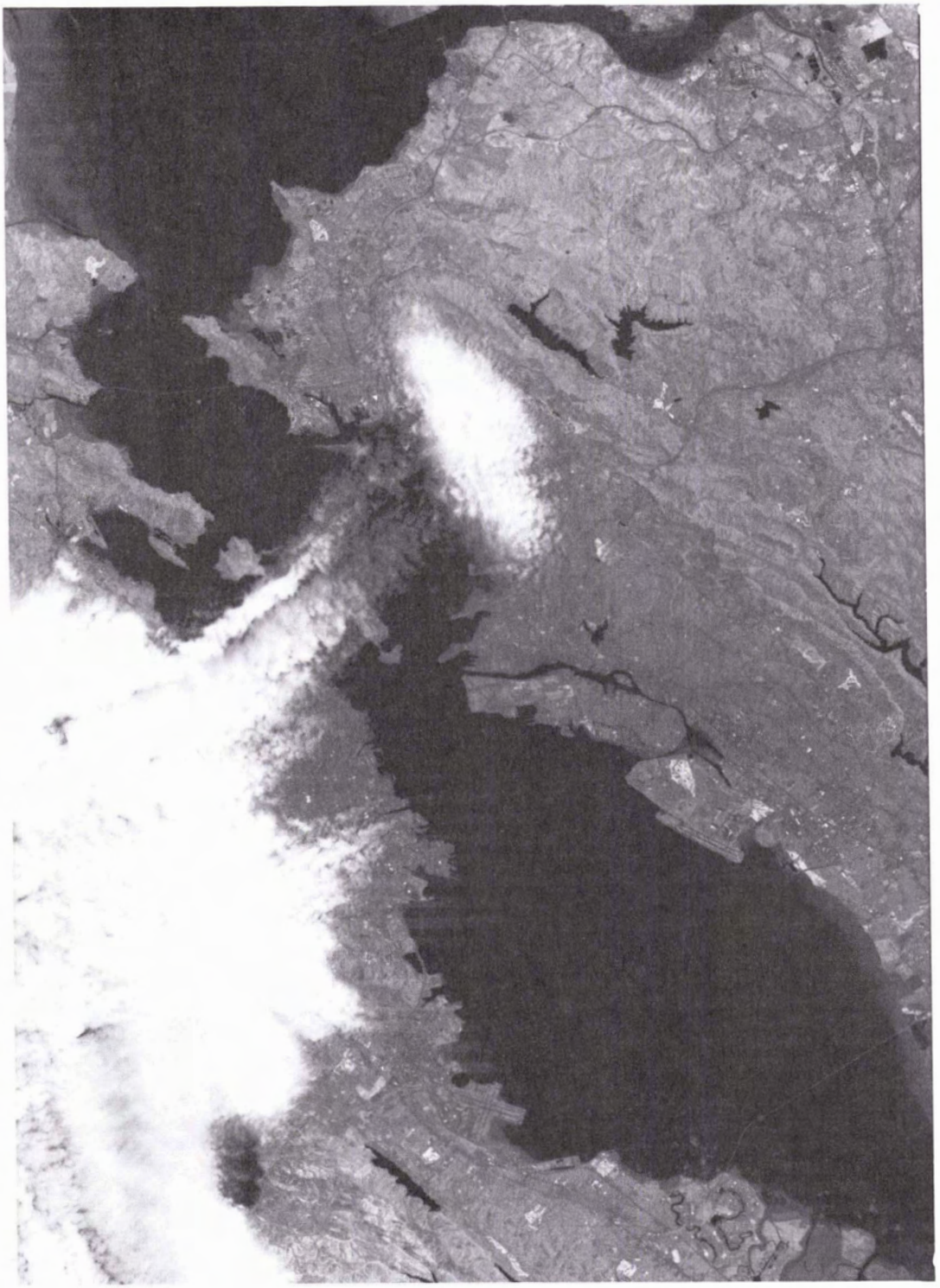

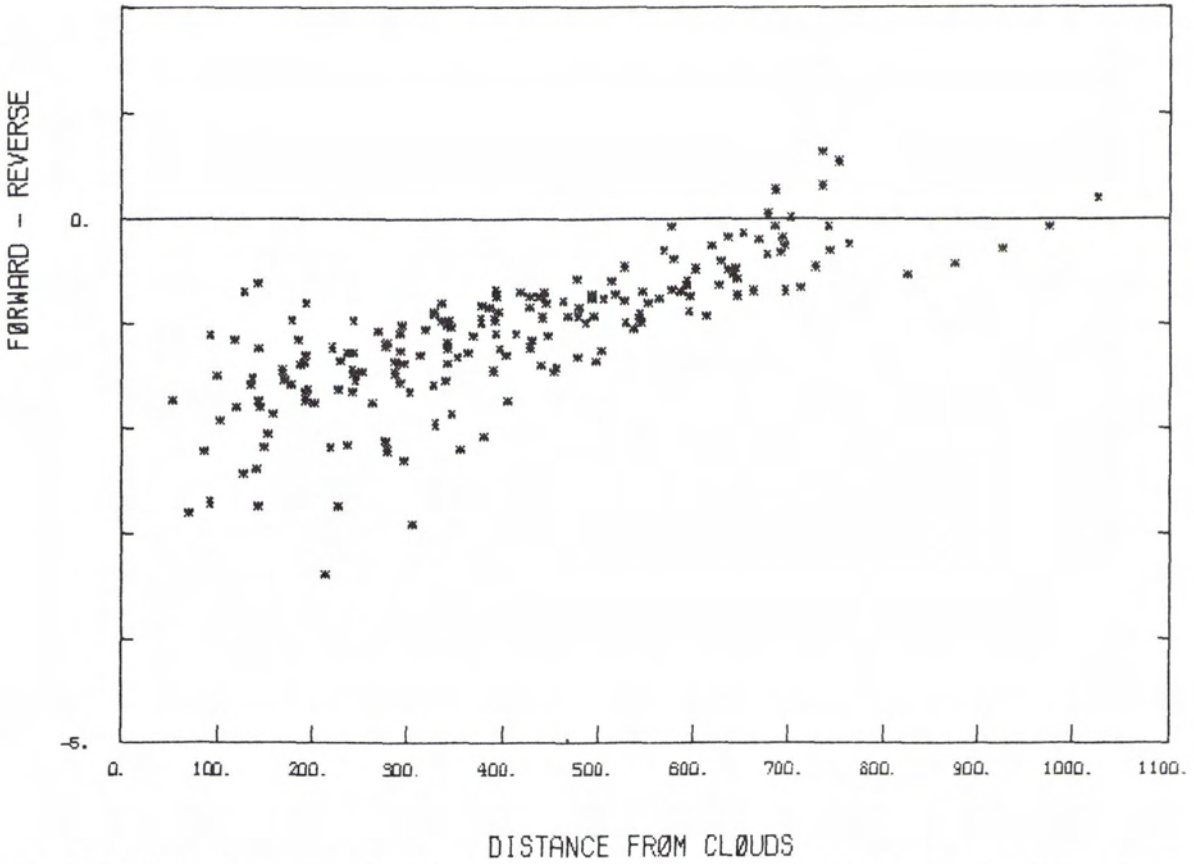

FIG. 6. Bright-target recovery delay. Differences in the average for all detectors in band 4 between adjacent forward and reverse scans in the south San Francisco Bay are shown as a function of the distance, in samples, to the edge of the large cloud to the west. Bands 2 and 3 have comparable form but smaller amplitude.

scan direction. This technique measures the high-frequency noise and is immune to drift, droop, and level shift, apart from quantization effects. For a simple bimodal discrete population, this measure of noise is a factor of 2/square-root (N) larger than the standard deviation, where N is the average number of consecutive occurrences in one state. For the night scenes we examined, this measure of noise is approximately the square root of 2 greater than the standard deviation of the data.

The resulting statistics for Landsat night subscenes are summarized in Tables 6 and 7. The dependence of noise upon scan direction for all detectors is negligible. Band 7, detector 7, of Landsat-4 TM shows a small effect in dark scenes, due to the influence of small level shifts on the proportion of clipping at zero. Another comparison of two Landsat-4 night scenes spaced 3 months apart showed little change, typically 0.1 DN, and less than 0.3 DN for all detectors. The noise of band 5, detector 10, of Landsat-5 is 1.0 DN greater than all other detectors in that band, due primarily to coherent noise exhibited by this detector. Measures of first-difference noise in areas of near-uniform radiance in day scenes (192 lines by 512 samples, in San Francisco Bay) are greater by 0.1 to 0.6 DN (band average) in the reflective bands and greater by less than 0.7 DN for all detectors.

By this measure of noise, the performance of the Landsat-5 TM is slightly better than that of Landsat-4: the Landsat-5 has an average of 0.25 DN less noise over all the reflective bands. These night

PLATE 3. Part of the San Francisco Bay area imaged by Landsat-5, band 4. The striping in the southern part of the bay is caused by bright-target recovery delay (BTRD), and decreases eastward from the edge of a large cloud. Although the small cloud east of the bay does not cause discernible BTRD, the lower contrast, but more extensive, land area east of the north part of the bay causes a small BTRD effect on the reverse scans.

TABLE 5. BRIGHT-TARGET RECOVERY DELAY MEASURED FOR LANDSAT-5 IN THE SAN FRANCISCO SCENE

Band	BTRD Magnitude (DN)	DN Level		
		Clouds	Land	Water
2	3.1	170	56	38
3	3.0	184	62	29
4	2.2	138	67	14

scenes are not thermally uniform, however, and the analysis provides only an upper limit on noise of the thermal band.

COHERENT NOISE

Fourier analysis on Landsat-4 TM scenes has revealed coherent noise (Bernstein *et al.*, 1984; Kieffer *et al.*, 1984). Two B-data subscenes, Cape Cod and Richmond, were selected for the current Landsat-4 analysis, both with starting line 1, starting sample 1025, with 512 lines and 1024 samples. The Richmond subscene, acquired at night, was used to determine coherent noise at the dark-current level. The Cape Cod daytime subscene, a large area of cloud-free ocean, provided a uniform flat-field target for study of coherent noise at brightness levels above dark current. For the Landsat-5 analysis, similar B-data subscenes were taken from the Harrisburg night scene and from two San Francisco Bay water areas; each subscene consists of 32 lines by 256 samples.

For all lines of the seven bands, a one-dimensional fast Fourier transform (FFT) was applied. The amplitudes of each Fourier component of the 32 scans in Landsat-4 subscenes were averaged for each detector. For the Landsat-5 analysis, only two scans of data were used in assessing coherent noise; however, in those cases where noise seemed to depend on a specific detector, the FFTs were computed for 12 scans in each subscene. Because uniform-radiance fields were used, amplitudes of all Fourier components can be attributed to either random or coherent noise (except zero frequency). Typical background-frequency amplitudes (averages of the FFT over all frequencies) due to random noise for both TM detectors, for both day and night data, fall within the range of 0.01 to 0.07 DN for all bands.

The FFTs exhibited several sharp peaks well above background noise levels (see Tables 8 and 9). In Landsat-4, the strongest, most consistent peak-to-peak amplitude coherent noise exists at 3.2 pixels/cycle and is evident in almost all detectors in bands 1, 2, 3, and 4. The noise is visible in areas of uniform radiance and appears as a grainy, high-frequency pattern, especially in bands 1, 3, and 4. The noise has a characteristic amplitude of 0.3 DN with a maximum, full-swing oscillation of 2 DN. Because this high-frequency coherent noise is approximately the same for the day and night scenes, it is assumed

TABLE 6. DETECTOR NOISE DETERMINED BY STANDARD DEVIATION OF HORIZONTAL DERIVATIVE, LANDSAT-4 THEMATIC MAPPER RICHMOND, VA; NIGHT SCENE B-DATA SUBSCENE 480 LINES BY 2560 SAMPLES

Dect	Band 1	Band 2	Band 3	Band 4	Band 5	Band 6	Band 7
16	2.47+	0.70	1.11	0.74	1.32		1.61
15	1.78	0.59	0.74	0.46	1.33		1.29−
14	2.02	0.58	0.94	0.43	1.35		1.81
13	1.59	0.63	0.77	0.36−	1.40		1.31
12	1.61	0.31−	0.70	0.63	1.42		1.63
11	1.82	0.51	0.54−	0.46	1.50		1.51
10	1.60	0.49	0.91	0.57	1.35		1.70
9	1.57−	0.50	0.65	0.39	1.44		1.55
8	1.90	0.74	1.36+	0.84+	1.34		1.52
7	1.96	0.56	0.77	0.43	1.80+		2.78+
6	2.09	0.81	0.82	0.78	1.48		1.67
5	1.57−	0.71	0.82	0.52	1.43		1.50
4	1.62	1.10*	1.14	0.64	1.43	2.14+	1.71
3	1.66	0.74	0.78	0.78	0.85*	1.99−	1.37
2	2.12	1.58+	0.82	0.64	1.30−	2.11	1.63
1	1.80	0.59	0.79	0.53	1.39	2.09	1.63
A	1.71	0.63	0.85	0.58	1.38	2.08	1.64
Raw Data, All Detectors							
Mean	2.72	2.32	2.46	2.26	2.62	117.48	2.45
Std. Dev:	1.12	0.54	0.64	0.45	0.85	8.85	1.01

Notation: A = Average of All Detectors, − = Minimum, + = Maximum
* = Detector Dead

TABLE 7. DETECTOR NOISE DETERMINED BY STANDARD DEVIATION OF HORIZONTAL DERIVATIVE, LANDSAT-5 THEMATIC MAPPER HARRISBURG, PA, NIGHT SCENE B-DATA SUBSCENE 480 LINES BY 2560 SAMPLES

Dect	Band 1	Band 2	Band 3	Band 4	Band 5	Band 6	Band 7
16	1.49	0.44	0.60	0.70+	1.37		1.41
15	1.19−	0.36	0.48	0.15	1.27−		1.18
14	1.55	0.22	0.49	0.40	1.34		1.48
13	1.32	0.40	0.58	0.18	1.41		1.14−
12	1.39	0.18	0.86+	0.34	1.53		1.51
11	1.27	0.28	0.50	0.25	1.28		1.31
10	1.40	0.15	0.46−	0.35	2.23+		1.42
9	1.23	0.21	0.73	0.20	1.32		1.22
8	1.59+	0.20	0.48	0.40	1.32		1.53
7	1.26	0.40	0.55	0.09	1.47		1.25
6	1.43	0.13−	0.48	0.29	1.33		1.54+
5	1.31	0.43	0.66	0.07−	1.30		1.22
4	1.58	0.29	0.63	0.13	1.45	0.79	1.42
3	1.47	0.45	0.74	0.30	1.35	0.78	1.32
2	1.48	0.63	0.51	0.19	1.30	0.72−	1.34
1	1.53	0.64+	0.84	0.66	1.30	0.84+	1.33
A	1.41	0.34	0.60	0.29	1.41	0.78	1.35
Raw Data, All Detectors							
Mean:	2.43	2.00	2.12	2.09	2.36	84.49	2.28
Std. Dev:	0.93	0.27	0.45	0.29	0.92	3.95	0.88

Notation: A = Average of All Detectors, − = Minimum, + = Maximum

to be an additive component to the signal and not a function of scene brightness. Coherent noise at 17.35 pixels/cycle is evident in almost all detectors of these same four bands (although much weaker in amplitude than that at 3.2 pixels/cycle) but was not found in the nighttime data.

In Landsat-5, a dominant spatial wavelength of about 12.0 pixels/cycle is present, with varying amplitude, in most detectors of bands 1, 3, 5, and 7. The band-average amplitude of this noise for bands 2 and 4 is at or below the background noise level. This noise shifts in period by 0.55 pixels/cycle between the day and night scenes. Band 5, detector 7, exhibits a relatively high peak-to-peak amplitude for this noise; the amplitude remains fairly constant within a particular scan and with respect to time, and is additive and not a function of scene brightness. The average amplitude is typically 0.6 DN with a maximum, full-swing oscillation of 5 DN. There is also a consistent peak-to-peak amplitude coherent noise at about 6.0 pixels/cycle. Although evident, with a range of amplitude, in most detectors of bands 1, 3, 5, and 7, it is much weaker than the 12.0 pixels/cycle noise. This weaker noise is probably the result of harmonic relation with the stronger 12.0 pixels/cycle noise.

In Landsat-4, an unusual coherent noise is present at or near 13.6 pixels/cycle in band 3, detectors 1, 3, and 9. Because the noise of the three detectors are so close in period, they are probably related. The visual appearance of this noise is a "stitching" pattern that occurs every 16th line. This noise differs in amplitude in the forward and reverse scan directions and changes over time. A noise-removal algorithm designed to track the phase and amplitude of the stitching pattern (Chavez and Soderblom, 1974) can remove most of this noise (Kieffer *et al.*, 1984).

The 4.7 pixels/cycle peak-to-peak amplitude coherent noise (Landsat-5, band 3, detector 12) remains fairly constant within a scan and over time; however, the daytime average amplitude is higher (0.4 DN compared with 0.2 DN), and the period is slightly shifted. The 14.22 pixels/cycle noise (Landsat-5, band 1, detector 4) is constant in period but varies slightly in amplitude, the average dark-current amplitude (0.3 DN) being 0.1 DN higher than the average daytime amplitude.

COMPARISON OF LANDSAT-4 AND LANDSAT-5 RESPONSES

Night scenes allow accurate determination of the zero-radiance offset of each detector. Determination of detector gain depends on either the stability of the internal calibration or independent measure of the radiance of a natural scene. A unique simultaneous observation by Landsat-4 and Landsat-5 has allowed a relative comparison of the two TMs. Acquisitions of the Birmingham scene by Landsat-4 and Landsat-5 occurred only 25 seconds apart. The longitude offset was about 630 samples, Landsat-5 being farther west by about 18 km. The responses of the two TMs to a common area were used to determine relative changes in gain and offset (the DN value for zero radiance) since the final pre-

TABLE 8. SUMMARY OF BAND-CONSISTENT COHERENT-NOISE LEVELS

Landsat-4	Band	1	2	3	4
Cape Cod Subscene					
3.26 pixels/cycle noise					
Band-average amplitude		0.28	0.06	0.10	0.13
Maximum amplitude		0.56	0.13	0.34	0.27
Detector with maximum amplitude		16	6	8	8
17.35 pixels/cycle noise					
Band-average amplitude		0.11	0.04	0.04	0.03
Maximum amplitude		0.18	0.08	0.10	0.09
Detector with maximum amplitude		4	1	1	12
Richmond Subscene					
3.23 pixels/cycle noise					
Band-average amplitude		0.46	0.08	0.13	0.11
Maximum amplitude		0.86	0.20	0.49	0.29
Detector with maximum amplitude		16	6	8	8
Landsat-5	**Band**	**1**	**3**	**5**	**7**
San Francisco Subscenes					
11.64 pixels/cycle noise					
North Bay					
Band-average amplitude		0.16	0.15	0.23	0.11
Maximum amplitude		0.28	0.26	0.66	0.24
Detector with maximum amplitude		4	5	7	8
South Bay					
Band-average amplitude		0.14	0.13	0.18	0.13
Maximum amplitude		0.24	0.20	0.60	0.30
Detector with maximum amplitude		10	5	7	10
Harrisburg Subscene					
12.19 pixels/cycle noise					
Band-average amplitude		0.11	0.07	0.18	0.10
Maximum amplitude		0.23	0.14	0.61	0.25
Detector with maximum amplitude		4	12	7	10

Band-average amplitude: Mean amplitude over all detectors in a band
Maximum amplitude: Maximum amplitude for a detector

TABLE 9. SUMMARY OF DETECTOR-DEPENDENT COHERENT-NOISE LEVELS

Landsat-4	Amplitude
Band 3, detectors 1, 3, and 9	
Cape Cod Subscene	
Detector 1 (13.83 pixels/cycle)	0.55
Detector 3 (13.62 pixels/cycle)	0.19
Detector 9 (14.22 pixels/cycle)	0.28
Richmond Subscene (all at 13.6 pixels/cycle)	
Detector 1	0.53
Detector 3	0.13
Detector 9	0.27
Band 3, detector 16	
Richmond Subscene (2.51 pixels/cycle)	0.12
Band 4, detectors 4, 8, and 10	
Richmond Subscene (2.62 pixels/cycle)	
Detector 4	0.13
Detector 8	0.14
Detector 10	0.09
Landsat-5	**Amplitude**
Band 5, detector 7 (11.64 pixels/cycle)	
North Bay	0.68
South Bay	0.61
Harrisburg (12.19 pixels/cycle)	0.61
Band 7, detector 10 (11.64 pixels/cycle)	
North Bay	0.23
South Bay	0.25
Harrisburg (12.19 pixels/cycle)	0.23
Band 3, detector 12 (4.74 pixels/cycle)	
North Bay (4.66 pixels/cycle)	0.33
South Bay	0.35
Harrisburg	0.23
Band 1, detector 4 (14.22 pixels/cycle)	
North Bay	0.19
South Bay	0.18
Harrisburg	0.29

Amplitude: the average amplitude computed over n scans for a particular detector

launch calibration. This check is independent of the internal calibration, and was performed on only the raw data. All these calculations ignore level shifts. The offsets and gains for Landsat-4 have a complex history (Barker, 1984), and the results of this comparison should not be extrapolated in time.

Areas of common coverage within quadrant 2 of the Birmingham scene were determined by registration of images from the two instruments at the four corner points of a rectangular area on the ground. Both image areas are rectangular and registered to within 3 pixels. The image areas are:

	Starting Line	Starting Sample	Number of Lines	Number of Samples	Number of Pixels
Landsat-4	128	32	2688	2304	6,193,152
Landsat-5	132	662	2688	2329	6,260,352

Band-wide histograms of the image areas were made for all bands, and the mean standard deviations, skew, and 2 percent and 98 percent levels computed. Skew did not differ significantly. The gains and offsets of the TMs were compared by a linear fit through the 2 percent and 98 percent points on the cumulative histogram using real interpolation to a fractional DN (Table 10). Gains and offsets were also compared by using the standard deviations of the common area. The deviations were in turn compared with the prelaunch ground-calibration values (J. Lansing, personal communication, 1984). Also compared were the relative offsets of two separate night scenes taken on different dates.

TABLE 10. COMPARISON OF LANDSAT-4 AND LANDSAT-5 RESPONSE.
HISTOGRAMS ARE OF AN AREA IN THE BIRMINGHAM SIMULTANEOUS COVERAGE COMMON TO BOTH LANDSATS. NIGHTTIME OFFSETS ARE FROM DATA IN TABLES 6 AND 7. PRELAUNCH DATA ARE FROM THE LANDSAT-4 TEST #5 AND THE LANDSAT-5 PRESHIP TEST.

	Band-Averaged Data Number						
Band	1	2	3	4	5	6	7
Landsat-4 Histogram							
2% point	60.85	22.55	20.67	28.38	36.10	122.51	12.86
98% point	84.02	38.47	47.58	71.80	119.69	145.90	57.40
mean	70.15	28.52	31.07	46.30	76.61	134.72	33.73
std. deviation	5.75	4.10	6.76	9.57	21.86	9.09	11.33
Landsat-5 Histogram							
2% point	65.04	24.40	22.35	28.85	35.11	98.66	12.64
98% point	88.98	41.59	51.65	73.71	118.99	108.76	57.00
mean	74.15	30.49	33.63	47.57	75.75	103.90	33.29
std. deviation	6.11	4.53	7.34	9.93	22.09	2.60	11.30
Landsat-4 offset							
prelaunch	0.8	0.8	−0.04	0.7	2.6		2.6
night scene	2.72	2.32	2.46	2.26	2.62		2.45
Landsat-5 offset							
prelaunch	1.9	1.6	2.0	2.0	3.1		3.2
night scene	2.43	2.00	2.12	2.09	2.36		2.28
Landsat-5 offset relative to Landsat-4							
prelaunch	1.1	0.8	2.04	1.3	0.5		0.6
night	−0.29	−0.32	−0.34	−0.17	−0.26		−0.17
Hist., 2% thru 98%	4.00	1.97	2.56	1.27	−1.14		−0.44
Hist., mean	4.17	1.82	1.63	0.45	−1.00		−0.21
Landsat-5 gain relative to Landsat-4							
prelaunch	1.0722	1.0299	1.0085	1.0184	0.9894		0.9759
Hist. 2% thru 98% slope	1.0331	1.0802	1.0892	1.0332	1.0036		0.9957
Std. deviation	1.0626	1.1049	1.0858	1.0376	1.0105		0.9974

In Landsat-4, the offsets of the warm focal plane bands changed significantly after launch; those of Landsat-5 changed less. The gain of Landsat-5 relative to Landsat-4 has increased in all reflective bands except band 1. Estimates of gain changes based on the standard deviation showed larger discrepancies than those based on extreme percentiles. The standard deviations were narrow, ranging from 4 to 11 DN (with the exception of band 5, which had 22 DN), and thus they may be strongly affected by the irregular ADC bin width. Histogram equalization that uses the standard deviation should be pursued for the TMs only with great caution.

Comparison of Landsat-4 and Landsat-5 fully corrected data (P-data) of this scene indicates inconsistencies of the internal calibration that average 5 percent for the six reflective bands (Metzler and Malila, this issue).

CONCLUSIONS

Current ground processing of Landsat products does not account for any of the imperfect characteristics discussed here and thus does not realize the full potential of the TM data. Most of these characteristics could be corrected by ground processing. Such corrections fall into several categories of increasing complexity: low-frequency corrections that are independent of scene content (ADC bin width and level shift), low-frequency corrections that depend on the general brightness of the scene (droop), intermediate-frequency corrections dependent on the detailed history of the scene scan (bright-target recovery delay and overshoot), and coherent noise. The most serious characteristic, judged by its appearance in fully corrected data, is level shift.

These corrections should be treated as floating-point (versus integer) additions prior to the radiometric equalization of all detectors. Availability of internal-calibration data simplifies correction for level shift and droop. Detailed recommendations on improvement of standard processing, based on analysis of Landsat-4, have been presented by Barker (1984) and Barker *et al.* (1984b).

In the absence of treatment of these corrections in standard product generation, a user interested in improved relative radiometry could readily correct for some of the more serious characteristics. Such correction would be especially useful for spectral categorization for small areas (less than one scan width in extent).

Correction can be accomplished on a band-by-band basis. A preliminary pass through the raw data is required to construct histograms for each de-

tector. The relative gain and offset of each detector can be determined on the basis of points near the extremes (e.g., 2 percent and 98 percent), incorporating the correction for ADC bin width. Using the band containing the detectors most sensitive to level shift (Landsat-5, band 5), one can also determine the level-shift state of each scan. The offsets for each detector can then be adjusted according to the level-shift sensitivity of that detector in proportion to the fraction of scans in the upper level-shift state. Two radiometric lookup tables are then constructed, one for each level-shift state, which incorporate the full ADC bin-width correction. If absolute calibration information is available, a corresponding correction to the slope and offset of the radiometric lookup table could be made at this point. The radiometrically corrected values are then generated by using the raw DNs and the appropriate lookup table for each detector based on the level-shift state of each scan.

Correction for droop, overshoot, and bright-target recovery delay requires more quantitative characterization than is presented here. If time-variant coefficients for these characteristics are not developed, an empirical correction could be made on an individual-scene basis.

Correction for coherent noise has been demonstrated only for areas of uniform radiance. The techniques described by Chavez and Soderblom (1974) and Bernstein *et al.* (1984) are similar in that they allow local adjustment to the amplitude and phase of the coherent noise. Successful application of these techniques to a complex TM scene remains to be demonstrated.

Although currently A-data, but not B-data, can be ordered for Landsat TM images, all of the corrections are more readily accomplished commencing with B-data. B-data would be more useful as an alternate standard product.

REFERENCES

Barker, J. L., 1984. Relative Radiometric Calibration of Landsat TM Reflective Bands: in *Landsat-4 Science Investigations Summary*, NASA Conference Publication 2326, Vol. I, pp. 140-180, and in *Proceedings Landsat-4 Science Characterization Early Results*, NASA Conference Publication 2355, Vol. III, pt. 2, pp. 1-220.

Barker, J. L., Abrams, R. B., Ball, D. L., and Leung, K. C., 1984a. Radiometric Calibration and Processing Procedure for Reflective Bands on Landsat-4 Protoflight Thematic Mapper: in *Landsat-4 Science Investigations Summary*, NASA Conference Publication 2326, Vol. I, pp. 90-91, and in *Proceedings Landsat-4 Science Characterization Early Results*, NASA Conference Publication 2355, Vol. II, pt. 1, pp. 47-86.

Barker, J. L., Gunther, F. J., Abrams, R. B., and Ball, D., 1984b. TM Digital Image Products for Applications: in *Landsat-4 Science Investigations Summary*, NASA Conference Publication 2326, Vol. I, pp. 116-119, and in *Proceedings Landsat-4 Science Characterization Early Results*, NASA Conference Publication 2355, Vol. II, pt. 1, pp. 147-220.

Bernstein, R., Lotspiech, J. B., Myers, H. J., Kolsky, H. G., and Lees, R. D., 1984. Analysis and Processing of Landsat-4 Sensor Data Using Advanced Image Processing Techniques and Technologies: *IEEE Transactions on Geoscience and Remote Sensing*, v. GE-22, no. 3, pp. 192-220.

Chavez, P. S., Jr., and Soderblom, L. A., 1974. Simple High Speed Digital Image Processing to Remove Quasi-Coherent Noise Patterns: *Proceedings, American Society of Photogrammetry Symposium*, Washington, DC, pp. 595-600.

Engle, J. L., and Weinstein, O., 1983. The Thematic Mapper—An Overview: *IEEE Transactions on Geoscience and Remote Sensing*, v. GE-21, no. 3, pp. 258-265.

Fischel, D., 1984. Validation of the TM Radiometric and Geometric Correction Algorithms: *IEEE Transactions on Geoscience and Remote Sensing*, v. GE-22, no. 3, pp. 237-242.

Fusco, L., Frei, U., and Hsu, A., 1985. Thematic Mapper: Operational Activities and Sensor Performance Results in ESA/Earthnet: *Photogrammetric Engineering & Remote Sensing*, (this issue).

Irons, J. R., 1984. An Overview of Landsat-4 and the Thematic Mapper: in *Landsat-4 Science Investigations Summary*, NASA Conference Publication 2326, Vol. I, pp. 62-67, and in *Proceedings Landsat-4 Science Characterization Early Results*, NASA Conference Publication 2355, Vol. II, pt. 1, pp. 15-46.

Kieffer, H. H., Eliason, E. M., and Chavez, P. S., Jr., 1984. Intraband Radiometric Performance of the Landsat 4 Thematic Mapper: in *Landsat-4 Science Investigations Summary*, NASA Conference Publication 2326, Vol. I, pp. 33-34, and in *Proceedings Landsat-4 Science Characterization Early Results*, NASA Conference Publication 2355, Vol. III, pt. 2, pp. 471-495.

Malila, W. A., Metzler, M. D., Rice, D. P., and Crist, E. P., 1984. Characterization of Landsat-4 MSS and TM Digital Image Data: *IEEE Transactions on Geoscience and Remote Sensing*, v. GE-22, no. 3, pp. 177-191.

Metzler, M. D., and Malila, W. A., Characterization and Comparison of Landsat-4 and Landsat-5 Thematic Mapper Data: *Photogrammetric Engineering & Remote Sensing*, (this issue).

National Aeronautics and Space Administration, 1984. *Landsat-4 Science Investigations Summary*, NASA Conference Publication 2326, Vol. I, 199 pp.; Vol. II, 174 pp.

———, 1985. *Landsat-4 Science Characterization Early Results*, NASA Conference Publication 2355, Vol. II (Thematic Mapper), 477 pp.; Vol. III (Thematic Mapper, continued), 593 pp.; Vol. IV (Applications), 448 pp.

Salomonson, V. V., and Koffler, R., 1983. An Overview of Landsat-4 Status and Results from Thematic Mapper Data Analysis: in *Proceedings 17th International Symposium on Remote Sensing of the Environment*, Environmental Research Institute of Michigan, pp. 279-291.

Santa Barbara Research Center, 1984. *Thematic Mapper: Design through Flight Evaluations, Final Report:* 203 pp.

Wrigley, R. C., Hlavka, C. A., Buis, J. S., and Card, D. H., Thematic Mapper Interband Registration and Noise Characteristics: *Photogrammetric Engineering & Remote Sensing*, (this issue).